

CONTENTS

OXIDE NANOMECHANICS	3
Oxides	3
Microelectromechanical Systems (MEMS)	4
OXIDE M/NEMS	5
Fabrication process for M/NEMS	6
Mechanical measurements of Oxide M/NEMS	12
Integration of oxides for multifunctional M/NEMS	21
Conclusions	22
Bibliography.....	23

This document reviews a selection of the results achieved during the H2020 OXiNEMS project (www.oxinems.eu). This is a live document and will continuously updated. This project has received funding from the European Union's Horizon 2020 research and innovation programme under grant agreement N.828784. This document is not a peer-reviewed paper.

Contact information: luca.pellegrino@spin.cnr.it

HISTORY:

- 08.02.2024 first version released

OXIDE NANOMECHANICS

OXIDES

We are all surrounded by oxides. Oxygen is the most abundant element in the Earth's crust and is highly reactive. This also means that many minerals are oxide minerals; oxides are employed to extract, for example, metals like iron. Many oxides are also of particular interest for their physical properties. Magnetite (Fe_3O_4) is a well-known magnetic (precisely a ferrimagnet) compound that has been employed in the ancient history for the fabrication of the first compasses. Silicon oxide, in its amorphous phase is used as insulating (dielectric) material in current transistors technology. In one of its crystalline phase, known as quartz, silicon oxide is employed as mechanical oscillator for clocks and timing components. Its status of crystalline material allows exploiting an important feature of quartz: piezoelectricity, or the properties to generate a voltage when deformed by an external pressure.

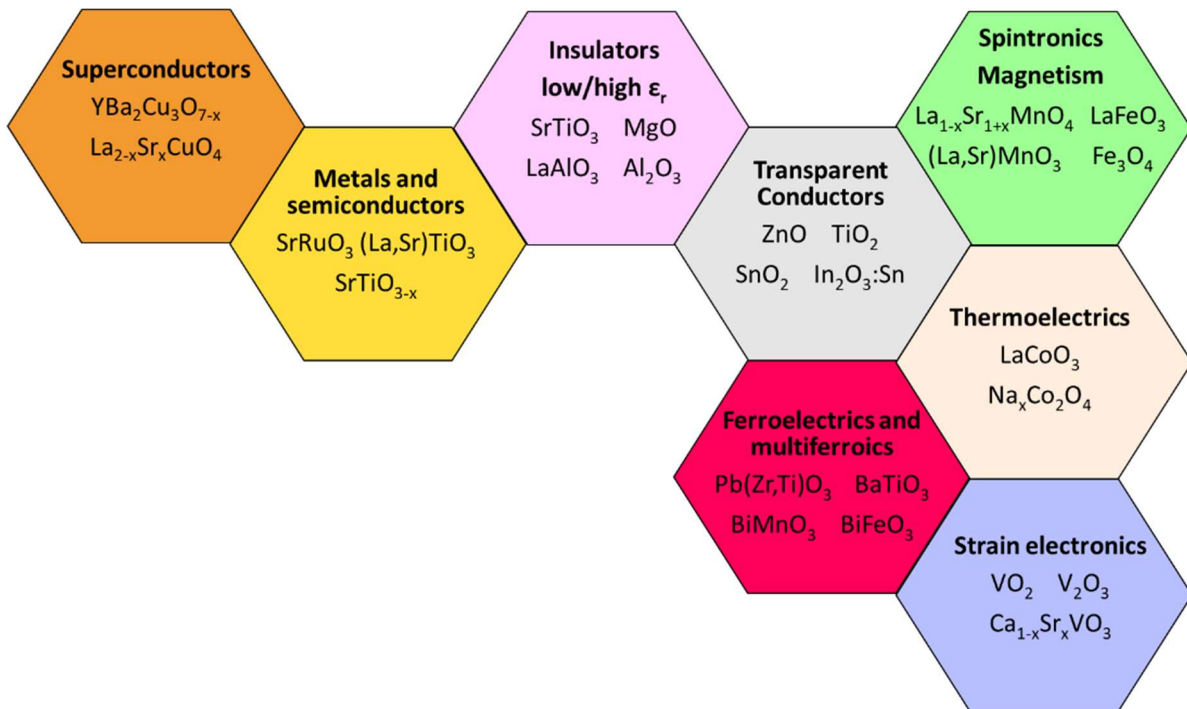


Figure 1 The world of oxide materials

The converse piezoelectric effect makes this material changing its shape when subject to an external voltage signal. Other oxide-based piezoelectric compounds, such as the well-known PZT, or $\text{Pb}(\text{Zr,Ti})\text{O}_3$, are used today in electronic devices and micromechanical components. Citing other peculiar properties of oxides, in 1986 some copper oxides were observed to be superconducting at high temperature. The most known compound used today is $\text{YBa}_2\text{Cu}_3\text{O}_{7-x}$ or YBCO - a complex oxide that has been widely employed for the realization of SQUID magnetometers working above the temperature of 77 K, the boiling point of liquid nitrogen.

Oxides may show changes of their properties with temperature. They can abruptly change their volume, their magnetic or electrical and optical properties. This aspect is of peculiar interest for developing sensors and mechanical actuators (devices that transform a source energy into a controlled force or mechanical motion) based on local changes of temperature. See, for example, the

micromechanical actuators based on Vanadium Dioxide previously developed by a collaboration between the SPIN institute of the National Research Council, the University of Genoa and Osaka University (www.vo2actuators.spin.cnr.it).

Oxides offer a broad panorama of useful properties (Figure 1)Figure 1. Some of them are already used in electronic devices – see for example indium tin oxide (ITO) in displays. Meanwhile, the research community is also active to finely control their physical properties in different forms, especially in micro and nanoscale artificial systems such as thin films and heterostructures (layers of different materials sandwiched), nanopatterned devices and nanoparticles. A roadmap on oxide electronics with different examples of oxide-based devices can be found on the review paper “Towards Oxide Electronics: a Roadmap”, Applied Surface Science Volume 482, 15 July 2019, Pages 1-93.

MICROELECTROMECHANICAL SYSTEMS (MEMS)

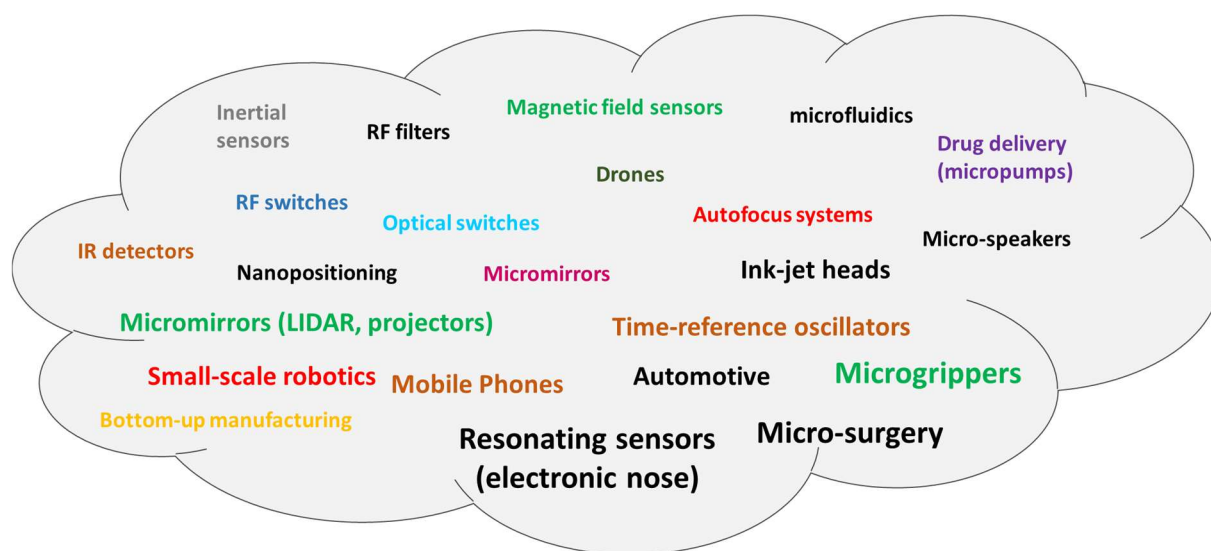


Figure 2 The MEMS world

In the OXiNEMS project, we are using oxides for the realization of small structures with designed roles as mechanical devices. Our idea is to enrich the field of Microelectromechanical Systems, also known as MEMS, with this class of materials and add more functional compounds to the existing materials library. The current MEMS field is broadly based on silicon technology. A paramount example is that of MEMS accelerometers and gyroscopes integrated in our mobile phones and tablet, but MEMS technology is also employed for the realization of microfluidic devices, infrared cameras, RF switches, oscillators, optical devices, microspeakers and microphones, pressure sensors, optical microdevices. Most of the MEMS devices require mechanical structures such as membranes, cantilevers or complex moveable parts clamped to the substrate by small joints, a sort of mechanical engineering at the microscale. Nano-Electro-Mechanical System (NEMS) take advantage of their extremely small dimensions to increase the sensitivity of mechanical-based resonant sensors. Despite different examples of NEMS sensors exist in literature, NEMS are mainly subject of research in the laboratories.

OXIDE M/NEMS

What we develop in OXiNEMS are basic mechanical structures with crystalline oxide thin films. We start from thin (about 100 nm of thickness) crystalline layers of oxides and then study how to fabricate moveable structures. To do so, we deposit these materials with a technique called Pulsed Laser Deposition and turn them into microstructures using optical lithography and selected chemical baths. One of the challenges in developing oxide-based micro and nanomechanical devices is the precise control of the internal stresses of these materials when grown as thin film. These crystalline oxides (a crystal is a periodic arrangement of atoms) are grown on a polished piece of another oxide crystal that works as “substrate”. The lattice of the grown oxide film is forced to match with the substrate lattice through a process called “epitaxy”. This matching may stretch or compress the film with respect to its own natural distances between the atoms (lattice parameters) with the result of having tensile-stressed or bent suspended structures, as it happens when stretching or wrinkling an elastic membrane by hands. The lattice parameters also depend on the precise ratio of the atomic composition of the oxide under study. A good example of such effect is $(\text{La,Sr})\text{MnO}_3$, a magnetic oxide that shows ferromagnetic state with a phase diagram that depends on the La/Sr ratio [i]. The La/Sr ratio in $(\text{La,Sr})\text{MnO}_3$ changes its lattice parameters and affects the stress with the substrate. We may grow $\text{La}_{0.7}\text{Sr}_{0.3}\text{MnO}_3$ or $\text{La}_{0.6}\text{Sr}_{0.4}\text{MnO}_3$ thin films on SrTiO_3 , a typical for oxide deposition, and detect different levels of stress on the produced structures.

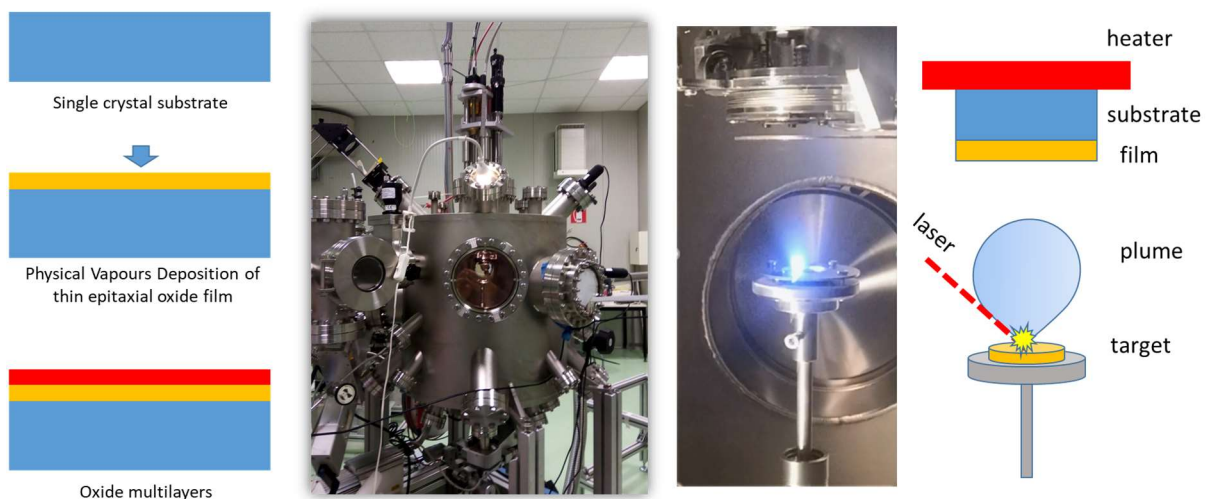


Figure 3 Pulsed Laser Deposition system @ CNR-Spin Genova

Pulsed Laser Deposition

Oxide films are made by Pulsed Laser Deposition, a versatile physical vapor deposition technique commonly employed for the fabrication of complex oxide thin films. The general principle of PLD is quite simple (**Figure 3**): a high-power pulsed laser beam (usually an excimer laser) is focused to a pellet (target) of the desired material located in a vacuum chamber. The laser beam evaporates ions, neutral atoms and species from the target in what is said “the ablation-plume”. In front of the target, at about 50 mm, is located a substrate where a film made of the elements and stoichiometry contained the target itself starts to grow. Composition of the target material is usually that of the wanted phase, but off-stoichiometric targets are sometimes prepared to compensate for evaporation of high volatility elements or resputtering from the film surface. The typical film growth rates are in the 0.01 nm/laser pulse range, about 100 nm/hour for a 3Hz pulse repetition rate. Good film crystal quality is achieved by tuning the different growth parameters. For example the substrate temperature, which is typically of few hundreds of degrees Celsius, the oxygen pressure in the chamber (for oxides growth), usually between 1 mbar and 10⁻⁶ mbar, the intensity of the laser, that can reach several hundreds of milliJoules per pulse, equivalent to few MW of power (the laser pulse duration is about 20 ns). Target-to-substrate temperature is also an important parameter to consider when depositing films by PLD.

FABRICATION PROCESS FOR M/NEMS

We are constantly developing fabrication protocols to realize suspended microstructures based on different complex oxides.

Generally, we start from an oxide thin film deposited on an oxide substrate by Pulsed Laser Deposition and prepare a photoresist mask using common photolithographic techniques such as optical lithography. We transfer the photoresist pattern to the film using physical or chemical etching. Physical etching is performed by ion milling technique: energetic Ar ions bombard onto the surface of the sample and progressively remove the oxide film areas that are not covered by the photoresist. Photoresist is removed by Ar ions too, but its thickness (about 4 microns) is higher than that of the film (about 0.1 microns).

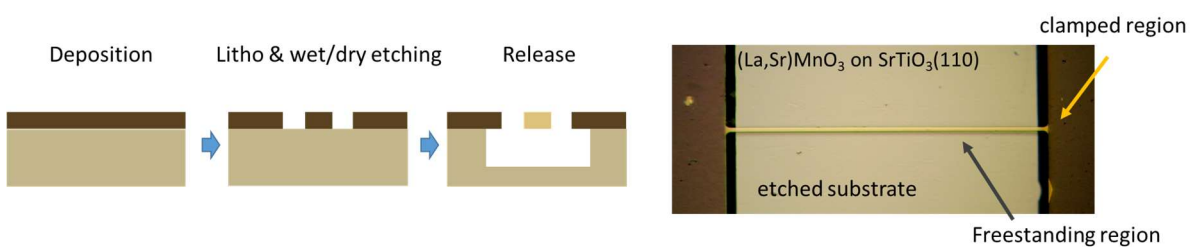


Figure 4 Fabrication processes of oxide M/NEMS: a micrometric pattern made from a (La,Sr)MnO₃ thin film is directly released from the SrTiO₃(110) substrate.

After the milling process, we remove the photoresist mask by solvents, leaving its replica onto the oxide film. Part of the substrate can be also removed during this process depending on the duration of the ion milling process. Ion milling is not selective and it removes all the materials, each one with different specific rates. Oxide films can be also etched by chemical methods and each composition has its own recipe. Regarding the suspension or release process, the removal of the oxide substrate regions under the patterned film is made using wet chemical etching. To do so, we explore the different sensitivity of oxides to chemicals. A typical example is that of manganite ((La,Sr)MnO₃)

thin films grown on strontium titanate (SrTiO_3 or STO) substrates: a $\text{HF}:\text{H}_2\text{O}$ solution removes SrTiO_3 , while it does not affect $(\text{La,Sr})\text{MnO}_3$. As an example, the picture of **Figure 4** shows a suspended microbridge structure made from a 100 nm thick magnetic oxide, called manganite or $(\text{La,Sr})\text{MnO}_3$. A patterned $(\text{La,Sr})\text{MnO}_3$ microbridge can be made freestanding by prolonged immersion in $\text{HF}:\text{H}_2\text{O}$ solution, because the acid progressively removes the portions of SrTiO_3 under the manganite pattern as evidenced in **Figure 5**.

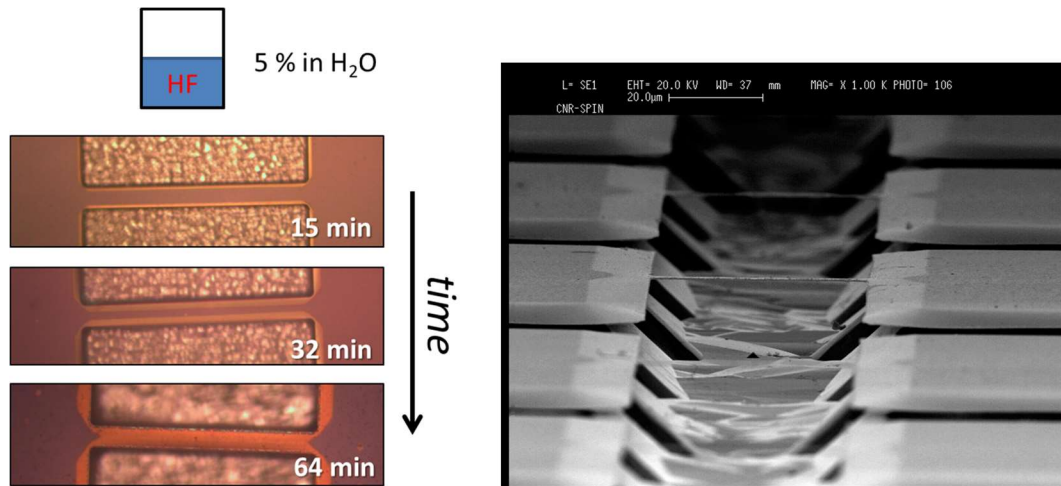


Figure 5 Progressive removal of the SrTiO_3 substrate under a $(\text{La,Sr})\text{MnO}_3$ microbridge grown on $\text{SrTiO}_3(001)$ and Scanning Electron Microscope image of a series of $(\text{La,Sr})\text{MnO}_3$ freestanding microbridges.

Instead, $\text{HCl}:\text{H}_2\text{O}$ solution removes $(\text{La,Sr})\text{MnO}_3$ but not SrTiO_3 ; $(\text{La,Sr})\text{MnO}_3$ sacrificial layers can be thus employed to fabricate freestanding SrTiO_3 thin film structures by prolonged immersion in HCl by patterning $\text{SrTiO}_3/(\text{La,Sr})\text{MnO}_3$ thin film heterostructures, **Figure 6** (see also reference [ii]). After chemical etching, the devices are rinsed in water and dried using Critical Point Drying method to avoid stiction.

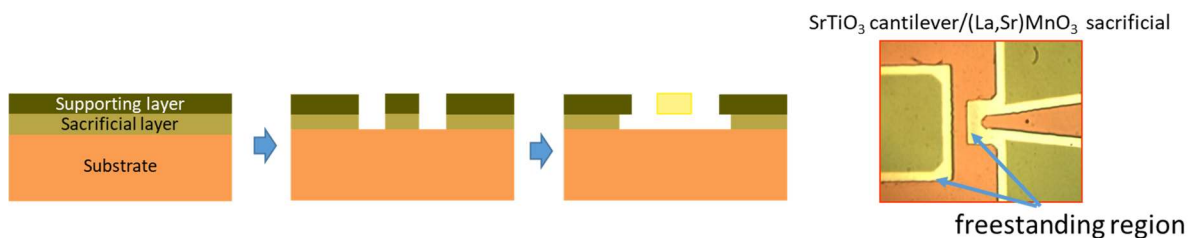


Figure 6 Fabrication processes of oxide M/NEMS: a SrTiO_3 pattern is released from the substrate using a $(\text{La,Sr})\text{MnO}_3$ sacrificial layer

We carefully studied the etching process of SrTiO_3 , one of the most used substrates for oxide deposition. STO single crystal substrates can be purchased with different crystal cuts, meaning that a crystal of STO is sliced into small $5 \times 5 \text{ mm}^2$ or $10 \times 10 \text{ mm}^2$ pieces (substrates) along some particular planes with respect to its cubic lattice. The etching rate of STO in HF solution strongly depends on the direction with respect to the lattice. This is not surprising as same phenomenology is well-known for silicon technology where –for example – the silicon etch rate in KOH depends on the crystal plane. In order to study the STO etching rate in HF and its dependence on the crystallographic direction, we performed a simple experiment: we realized squared masks (masks were made by a patterned 50 nm thick LSMO film, but this is a detail) on SrTiO_3 substrates having three crystallographic directions, namely $\text{STO}(100)$, $\text{STO}(110)$, $\text{STO}(111)$. We then immersed the samples

in the HF 5% water solution kept at 30 °C. At given times (1, 2, 5, 10, 20, 40, and 60 min), we removed the samples from the bath, cleaned in deionized water, dried under nitrogen flow, and inspected at the optical microscope and optical profilometer. The difference between the samples is clearly observable in **Figure 7**, where the profile of the three substrates is measured after 1 hour immersion in HF 5% water solution.

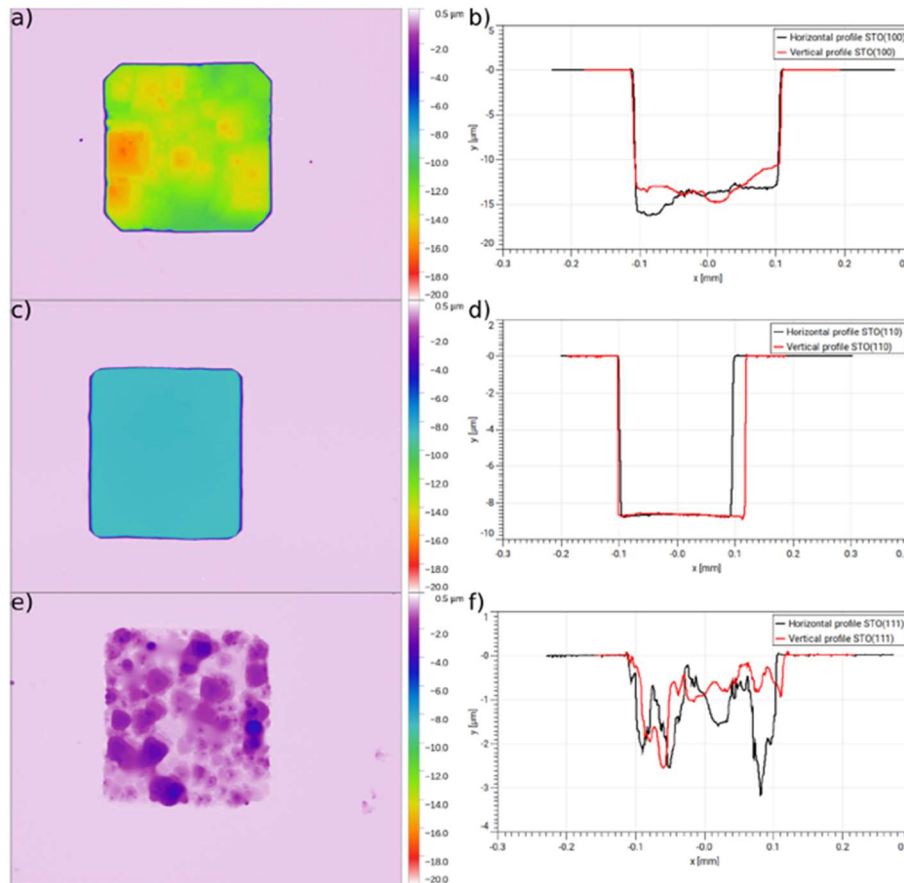


Figure 7 The etching of SrTiO₃ substrates with three different crystal cuts: SrTiO₃(100), SrTiO₃(110), SrTiO₃(111). Adapted from Appl. Phys. Lett. 19 July 2021; 119 (3): 033504. <https://doi.org/10.1063/5.0056524>

Apart from the different etching rate of the three orientations reported in **Table 1**, we observe a significant different roughness of the etched surfaces among the three samples. The roughening of the surface is due to the formation of etching pits that progressively cover all the surface. Surprisingly, the STO(110) substrate remains pretty flat even at the end of the etching process with a *rms* roughness of about 4 nm, as measured by AFM, with no detectable pit formation (see the supplementary material, Sec. II of A. Plaza et al.). Such striking difference shows, in accordance with previous literature reports, that pits that form on this surface are not able to survive by their own and rapidly disappear contributing to the etching mechanism. The overall out-of-plane etching rate on a large scale (several tens of micrometers) is a combination of different processes, also including the evolution of the pits and is described in details in reference A. Plaza et al. [iii]. Another important aspect of the previously cited work is a systematic study of the three-dimensional geometry of freestanding oxide microbridges fabricated on STO substrates. We analyzed the evolution of the underetching below 100 nm thick LSMO microbridges and the geometry of the underetch profile around their clamping regions for the three different substrate types and microbridge directions.

Optical inspection of the bridges after a given amount of etching time reveals the importance of choosing the proper substrate and also the design and orientation of the pattern (**Figure 8**).

SrTiO ₃ wet etching		
Etching Direction	Depth after 1 hour in HF 5% (2.8M) @30 °C	Surface roughness
[001]	13.5 μm	1 μm
[011]	9 μm	4 nm
[111]	0.6 μm	0.75 μm

Table 1 Vertical etching rate for SrTiO₃ substrates with a given crystal cut

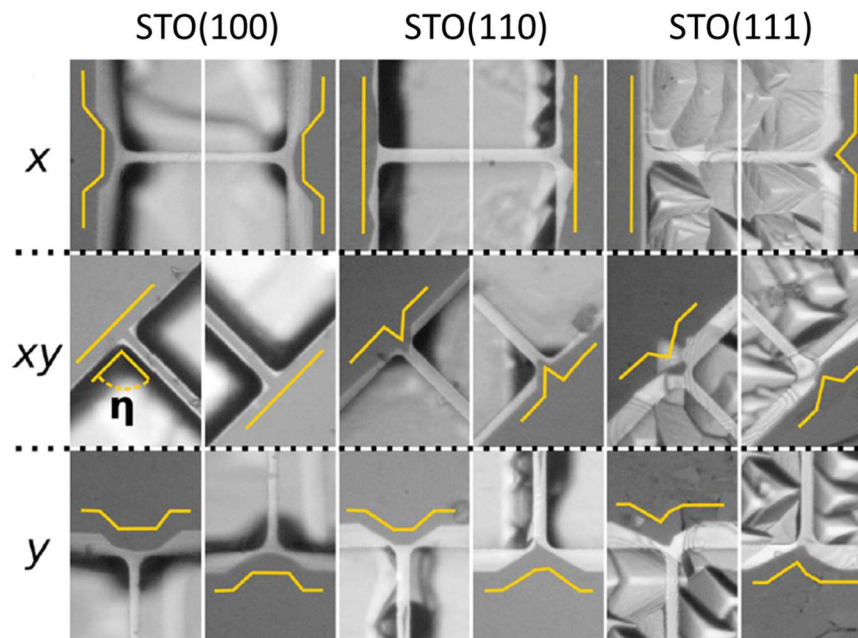


Figure 8 magnified details of the clamping area of LSMO freestanding microbridges fabricated along three different planar directions (0°, 45° and 90°) and on three different crystal orientations (SrTiO₃(100), SrTiO₃(110), SrTiO₃(111)). Adapted from Appl. Phys. Lett. 19 July 2021; 119 (3): 033504. <https://doi.org/10.1063/5.0056524>

Microbridges fabricated on STO(111) are freestanding but the etching depth is so low to hinder the realization of mechanical resonators. Microbridges fabricated on the other two substrates are suited for making well-suspended (>10 μm deep) resonators provided we consider the following main points. 1) Microbridges fabricated on STO(110) have different geometries for the clamping regions depending on their orientation on the substrate plane (0°, 45°, 90°). 2) Microbridges fabricated on STO(100) show 90° symmetry (x and y directions give similar results), meaning unchanged shape of the clamping region; bridges fabricated along the 45° direction need significantly large amount of etching time to be fully suspended.

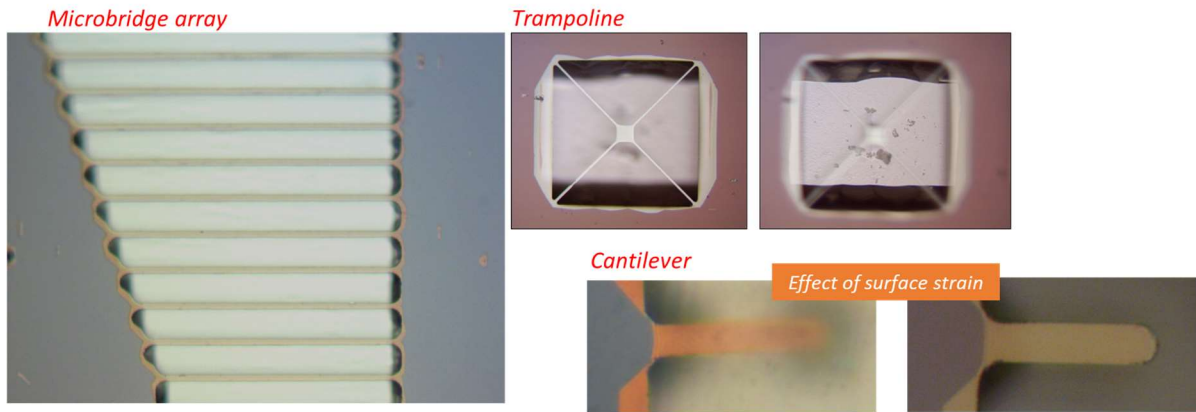


Figure 9 LSMO freestanding microbridge array, cantilever and trampoline. The two LSMO cantilevers have different strain gradients as evidenced by the defocused image of the cantilever to the left. The image of the LSMO trampoline is taken focusing on the LSMO film (left) and on the STO(110) etched surface (right).

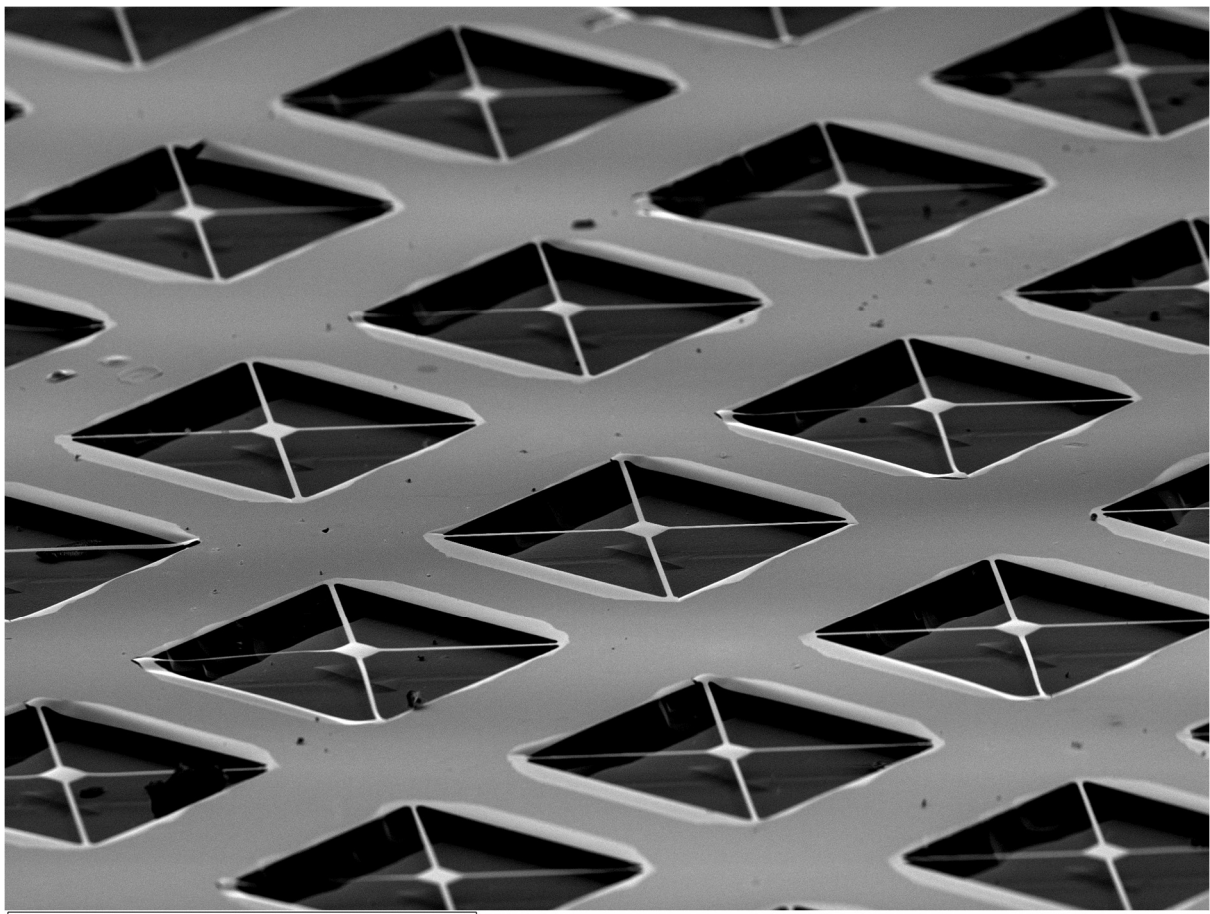


Figure 10 Scanning Electron Microscope image of an array of trampolines fabricated starting from 100 nm thick epitaxial (La,Sr)MnO₃ film grown on SrTiO₃(110).

Once more, our studies showed that besides the materials, the design of the two-dimensional geometry of the MEMS patterns is an important step for the final three-dimensional geometry of the micromechanical devices with important consequences on their mechanical behavior. In the following section, we will show some examples of freestanding oxide structures realized on STO substrates (Figure 9 and Figure 10) considering the above mentioned points.

The etch process reaction between HF and STO produces residues that attach to the surface (**Figure 11**) and cannot be easily removed by sonication of the sample because ultrasounds would unavoidably damage the MEMS device. To decrease the amount of residues, we perform etching by slightly heating the solution (this to create convective flow) and by mild agitation using a magnetic stirrer. The speed of the magnetic stirrer cannot be too high, as the drag forces would break the MEMS structures as well. Our analysis on the white deposits show that these residues contain fluorine and, in most of the cases, we see cubic crystallites identified as SrF₂. SrF₂ is not soluble in water and its accumulation prevents or slow down the further etching of the substrate. Immersion of the oxide samples in 8.5 % H₃PO₄: water solution for 1 hour greatly improves sample cleanliness.

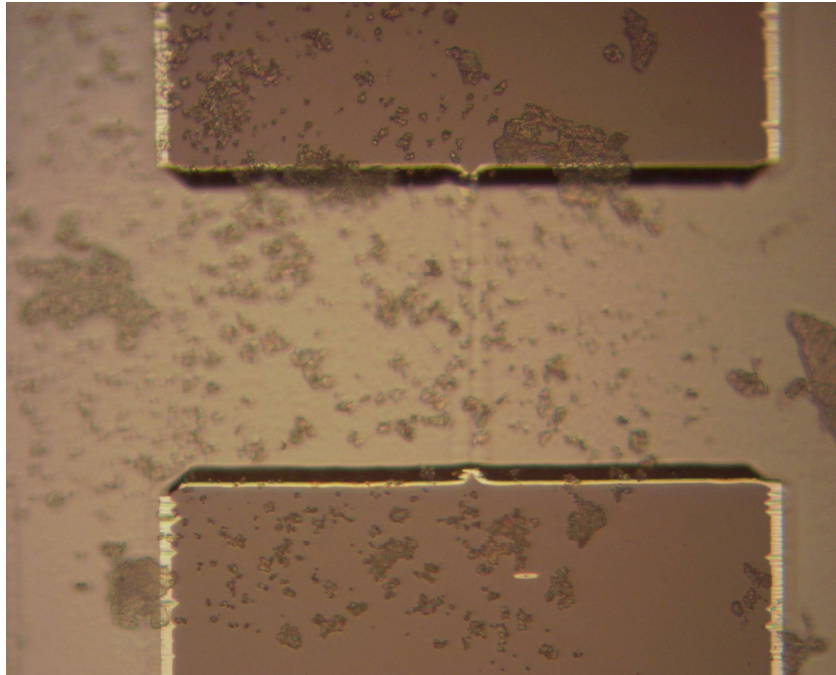


Figure 11 optical microscope image of a patterned structure (bridge broken) showing the presence of residues

In the OXiNEMS project, we also investigated other oxide materials to broaden the spectrum of applications also with a view to fabricating M/NEMS devices employing thin film oxide bilayers, and generally freestanding oxide heterostructures with multifunctional layers. The materials that we mostly considered are reported in **Table 2** with a short text explaining their main functionalities.

Material	Main Role
SrTiO_3	dielectric/structural layer
$(\text{La,Sr})\text{MnO}_3$	magnetic/structural layer
LaAlO_3	dielectric/structural layer
EuTiO_3	dielectric/structural layer
$\text{YBa}_2\text{Cu}_3\text{O}_{7-x}$	superconducting layer

Table 2 Main oxide materials investigated in the OXiNEMS project

Together with VO_2 and SrRuO_3 that have been developed by our group in other projects, we might consider these oxides as “brick” for the oxide nanomechanics and their characterization somehow the basis for building complex mechanical structures where “stress engineering” and the response to external stimuli or ambient conditions are elements of value for enriching the capabilities of the M/NEMS field.

MECHANICAL MEASUREMENTS OF OXIDE M/NEMS

Fabrication of an oxide freestanding structure is the first exciting step in the realization of a M/NEMS device. These tiny structures suspended over a micrometric air gap above the substrate are a wonderful landscape for the curious eye of a researcher playing with the incomparable direct view from an optical microscope. But this is just the beginning, as these structures might bend depending on the internal stresses and vibrate at frequencies generally well above the audible acoustic range. These static and dynamic mechanical features of the M/NEMS devices are well correlated to the intrinsic physical properties of the oxides they are made of.

STATIC BENDING OF OXIDE FREESTANDING STRUCTURES

In OXiNEMS, we characterized different freestanding oxide structures having selected geometries. When we release an oxide film grown compressed over a selected substrate, its final shape is deformed. For example, a long microbridge is not flat anymore, but it bends upward or downward. The total curvature and so the length of the microbridge itself are proportional to the amount of compressive stress of the film. A paradigmatic and manifest example of this has been reported for VO_2 films across their structural transition at around 68°C by our group [iv]. We detected compressive stress also with EuTiO_3 (ETO) thin films grown on top of SrTiO_3 substrates. ETO is a well-known complex oxide mainly investigated for its magnetic properties and its incipient ferro-electricity. ETO has pseudo-cubic lattice structure with a reported values at 300 K in between 3.860 and 3.908 Å. ETO perfectly grows cube-on-cube over SrTiO_3 and microbridges and cantilevers can be fabricated using selective etching in HF solution.

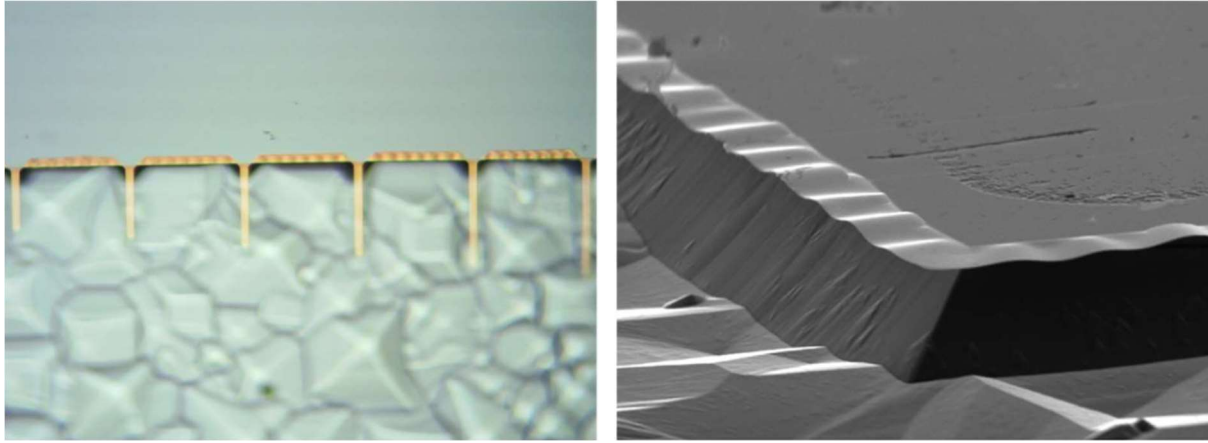


Figure 12 Optical image of a series of cantilevers fabricated starting from a EuTiO_3 film grown on $\text{SrTiO}_3(100)$ substrate. The small compressive strain detected in some film samples is evidenced in the undulating structures at cantilever base and the SEM image of the pattern borders, where the freestanding film can be observed.

A first look to the optical microscope shows slightly bent cantilevers and microbridges, as the structures results slightly out from the focal plane in some parts. In some cases, we observe “wavy” structures at the freestanding borders that are natural consequence of the underetching process (**Figure 12**). We employed an optical interferometer to analyze more quantitatively the final shape of the thin film patterns after the release process. This instrument is an interferometric microscope providing a height map of its field of view and measures the three-dimensional shape of a reflecting object, here our oxide structures. We could detect and quantify the curvature of both cantilevers and microbridges fabricated on a $5 \times 5 \text{ mm}^2$ substrate and calculate for each structure the amount of compressive stress and model it with some assumptions [v]. A simple model assumes that all the compressive stress is converted into strain when the structure is released. With this model, the amount of strain is calculated dividing the total measured length of the microbridge by the nominal length of the microbridge, i.e. its length if it would be straight (**Figure 13**). We performed this analysis on 140 microbridges having about 100 nm thickness and fabricated across the entire film. The calculated average strain of $\epsilon = +0.14\% \pm 0.02\%$ indicates an in-plane lattice compression of about 0.55 pm. We attribute the observed compressive stress to the formation of thermodynamically stable defects during the growth, such as oxygen vacancies or dislocations. The strain value calculated for the each bridge is slightly different and changes following long-range film inhomogeneity likely due to small variations of the film stoichiometry, a process that typically occurs with Pulsed Laser Deposition. The mechanical measurements of EuTiO_3 cantilevers give other important information on the material properties. For example, cantilevers can be employed to evaluate the strain gradient in the out-of-plane direction of the film. Cantilevers have a free end and strain is thus ideally relaxed. But if the film is not perfectly homogeneous, a small change of stress along its thickness results in a vertical bending of the microstructure.

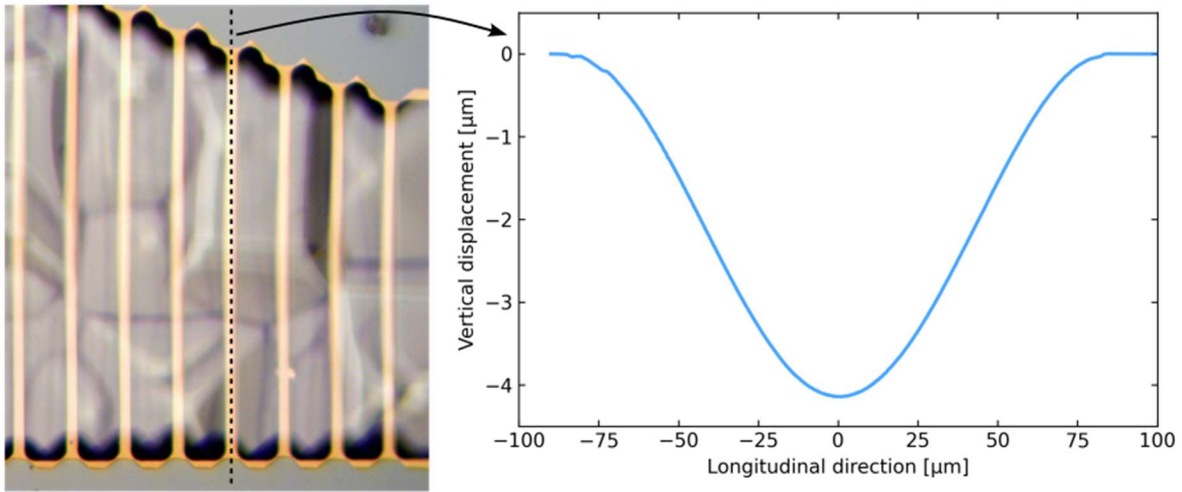


Figure 13 Curvature of a EuTiO_3 microbridge measured by optical profilometry. Extracted from Nicola Manca et al. "Strain, Young's modulus, and structural transition of EuTiO_3 thin films probed by micro-mechanical methods" *APL Mater.* 11, 101107 (2023) [v]

. The strain/curvature relation of a thin foil or structure is an interesting aspect when developing thin freestanding oxides. A small stress gradient results in a large change of curvature and so in a large vertical displacement of the cantilever (**Figure 14**). Conversely, thin structures can bend a lot before achieving the maximum allowed stress before fracture takes place.

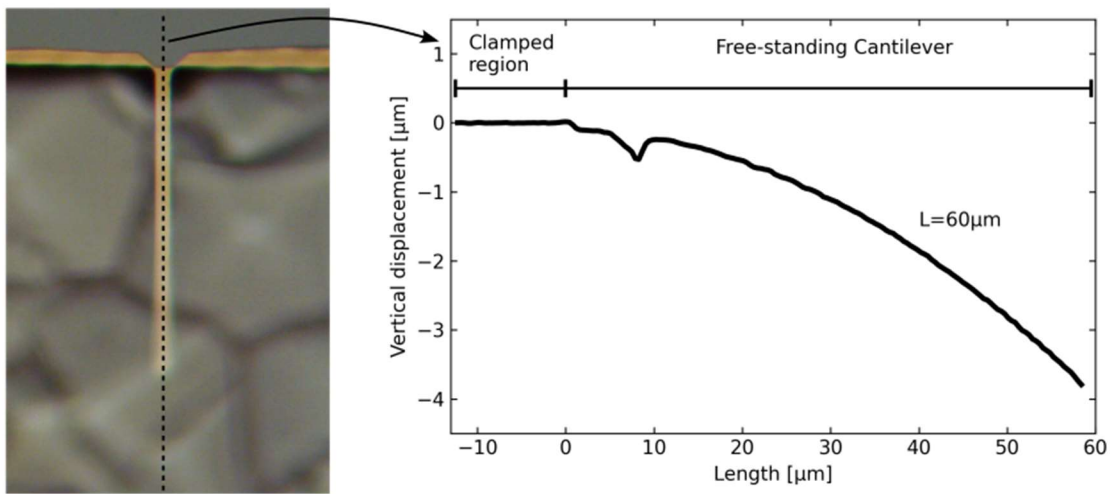


Figure 14 Curvature of a EuTiO_3 cantilever measured by an optical profilometer. Extracted from Reference [v].

By measuring the bending profile of ETO cantilevers, we were able to make a simple model and evaluate a "strain gradient" across the film thickness leading to a difference in strain between the bottom and top surface of about 0.023 %, about six time smaller than the average in-plane strain. If the strain gradients are too high, the cantilevers curl too much for making a classical dynamic measurement of their resonance frequency similarly to what is done in Atomic Force Microscopy.

DYNAMIC CHARACTERIZATION OF OXIDE RESONATORS

ETO microcantilevers can be measured with an optical lever setup (Figure 15) because ETO grown on STO has a low stress and stress gradient values and so they are slightly bent.

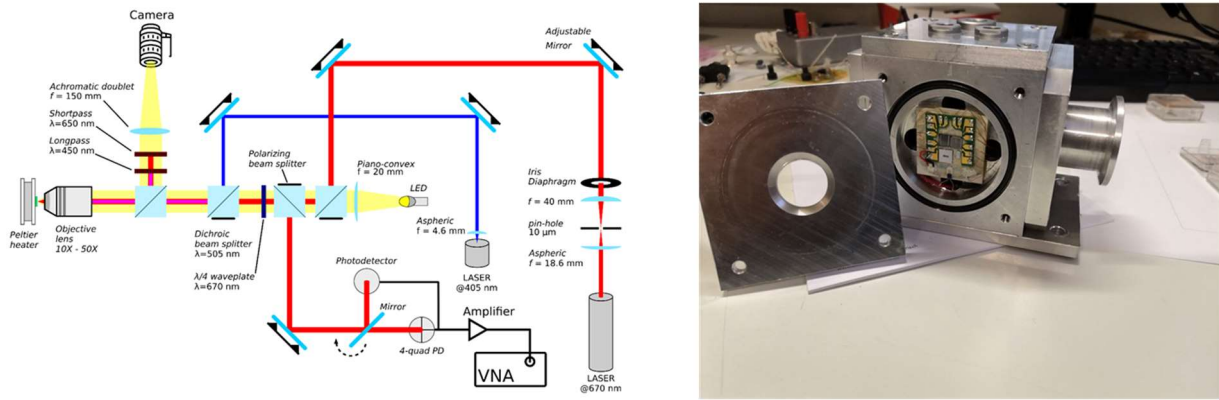


Figure 15 Scheme optical lever setup used for the characterization of Oxide M/NEMS around room temperature and picture of the sample holder.

Figure 16 shows the mechanical spectrum of a 75 μm-long ETO cantilever having 100 nm of thickness. The sample is set vibrating using piezoelectric element attached to the sample holder and the vibrations transmit to the cantilevers.

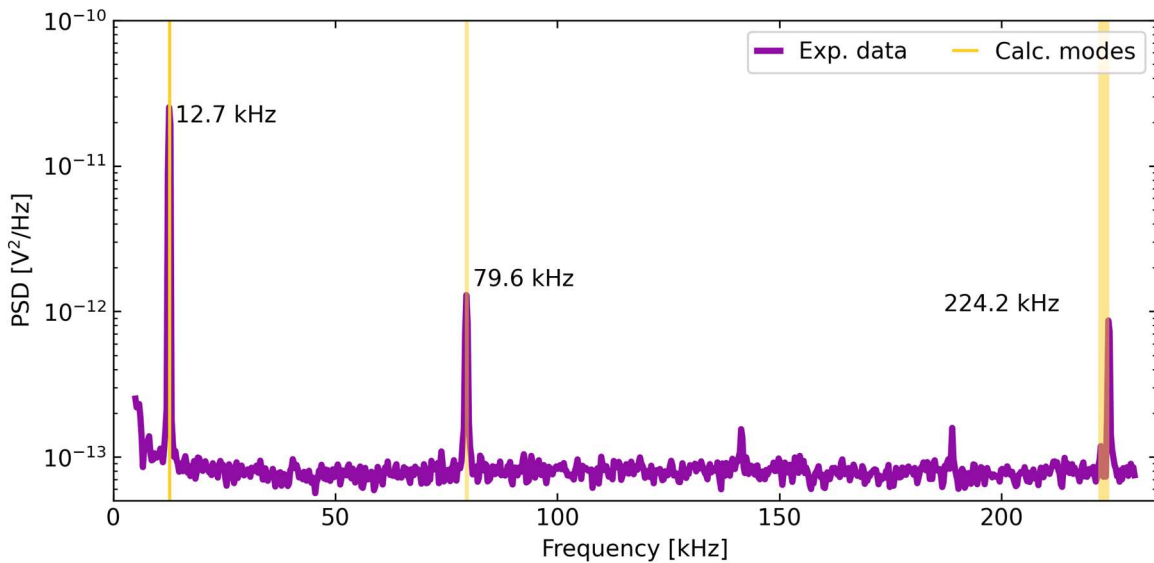


Figure 16 Mechanical spectrum of a ETO cantilever. Extracted from reference [v].

The observed spectrum is nothing less than the movement of the probed point (here the cantilever end) as a function of the frequency of the periodic mechanical excitation. In reality, the optical lever system detects the inclination of a movable structure, while the vertical displacement would be measured by an interferometer. However, the onset of mechanical resonances in the cantilevers can be detected with both the instruments.

The three observed peaks corresponds to the first three flexural modes of vibration of a simple cantilever and their value, in terms of frequency, can be fitted to a simple model using the Euler-Bernoulli theory.

Optical lever setup

The MEMS characterization setup located in the CNR-SPIN lab at the University of Genoa Physics Department has been designed to allow for concurrent electrical and mechanical measurements in controlled atmosphere and temperature. The setup is made of three main components: Optical system, Sample holder, Readout electronics.

The **optical system** consists of a continuous wave 670nm (red) laser and a pulsed 405nm (blue) laser. The first one is meant to probe the motion of the micro-mechanical devices, while the second is employed as a localized heat source. The optics mainly manipulates the red lasers to optimize the readout performances:

- *A spatial filter produces a non-diverging beam having Gaussian profile;*
- *Neutral density filters allows to control the laser power from 7mW down to 2nW while keeping the source at the output power where noise is minimal;*
- *An optical isolator (polarizing beam-splitter + $\lambda/4$ wave-plate) maximizes the intensity of the light coming back from the sample and sent to the detector;*
- *The dichroic beam splitter mixes red and blue light in the same optical path without intensity loss.*
- *An objective lens focuses the laser on the sample down to $1\mu\text{m}$ spot size and is also employed to observe the sample by a USB camera.*
- *The reflected light is sent to a photo-detector (single or four-quadrant) converting the light into an electrical signal (see later).*

The **sample holder** consists of a custom vacuum chamber designed by us. Its main characteristics are the following.

- *Base pressure 2×10^{-5} mbar*
- *Working temperature range is from -20°C up to 130°C .*
- *12 DC electrical lines and 4 coaxial cables, all of them can be independently connected to the sample by ultrasonic wire bonding.*
- *Three piezoelectric elements providing acoustic excitation. Each of them has a different cut-off frequency (900 kHz, 2 MHz, 8 MHz).*
- *Motorized XYZ stage having 12 mm travel length and $0.1\mu\text{m}$ step.*

The **readout electronics** comprises a high-bandwidth four-quadrant photo-diode developed within the OXiNEMS project. It is designed to work from DC up to 20MHz and its first version is in use for testing purposes. We are currently developing a second version with our project partners aiming to be released to the public.

Our setup also employs commercial data acquisition systems:

- *HP4395A Vector Network Analyzer operating from 10 Hz to 500 MHz with resolution bandwidth spanning from 2 Hz to 1 MHz*
- *HF2LI 50 MHz Lock-in Amplifier working from DC to 50 MHz at 210 MSa/s and 14 bits.*
- *Keithley 2450 Sourcemeter for four probe electrical resistance.*
- *LabVIEW interface for data acquisition and control over all the experimental parameters*

The resonance frequency of the flexural modes (f_n) of our cantilevers is modeled assuming thin and long beams having width much greater than their thickness (plate approximation) and is:

$$f_n = \frac{\lambda_n^2 t}{2\pi L^2} \sqrt{\frac{E}{12\rho(1-\nu^2)}}$$

Equation 1: $\lambda_n = \{1.8751, 4.6941, 7.8548, (2n - 1)\pi/2\}$ is a numerical parameter related to the mode shape, t is the thickness, L the length, ρ the density, and E the Young's modulus. (E gives a rapid outlook on the elastic behavior of a linear elastic material and is the ratio between the force per unit area and the axial strain of a slab of a given material), ν is the Poisson's number.

Remarkably, no stress dependence enters into **Equation 1**, but the Young's modulus enters and can be directly extracted from our experiments. The E value we obtain is 132 GPa, which is one-half of what other group reported on single crystals using a different method [vi].

In our work "*Stress Analysis and Q-Factor of Free-Standing (La,Sr)MnO₃ Oxide Resonators*" [vii], we study microbridges realized starting from 100 nm thick $(La,Sr)MnO_3$ (LSMO) films. LSMO grows with tensile strain on top of the SrTiO₃ substrate and thus LSMO microbridges vibrates as the strings of a guitar with resonance of the first flexural mode f_1 given by the following **Equation 2**.

$$f_1 = \frac{1}{2L} \sqrt{\frac{\sigma}{\rho}}$$

Equation 2: σ is the film stress, L the microbridge length and ρ the LSMO mass density.

This "string" limit is valid for highly stressed microbridges, as the represented case. Measurement of the microbridge frequency thus gives a rapid information of the stress state of the film in the area where the microbridge is fabricated. From the mechanical spectra as that reported in **Figure 17**, and inverting **Equation 2** we can calculate the stress level σ , which attains to about 260 MPa. A "stress map" of the film can be thus achieved and correlated with other physical measurements to extrapolate useful information as for example the homogeneity of the deposition process.

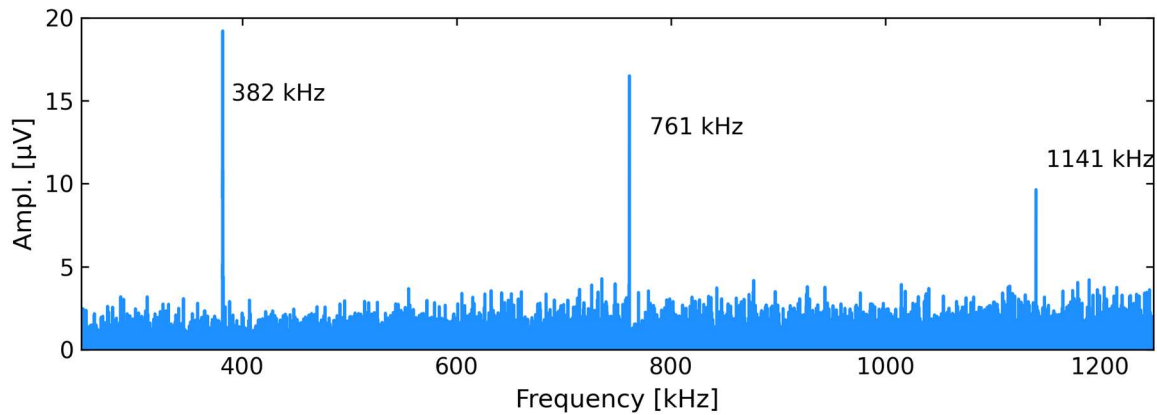


Figure 17 Mechanical spectra of a LSMO microbridge. Extracted from reference [vii].

If interesting mechanical properties - such as the Young's modulus - can be extracted by dynamical measurements of the microresonators, oxide-based M/NEMS show their peculiar behavior when changing the external parameters. Temperature is an important quantity in determining the phase of oxides. Changes of temperature can turn a conducting oxide into a superconductor (YBCO) or an insulator (VO_2) or even drive ordered states such as ferromagnetism (LSMO) or ferroelectricity (PZT, BTO). In the case of ETO, we measured the value of the first flexural mode of a cantilever as a function of temperature. We detected an anomaly of the frequency vs temperature nearby its anti-ferro-distortive transition and interpreted this as a concomitant change of the value of the Young's modulus with the transition in accordance with other authors (**Figure 18**).

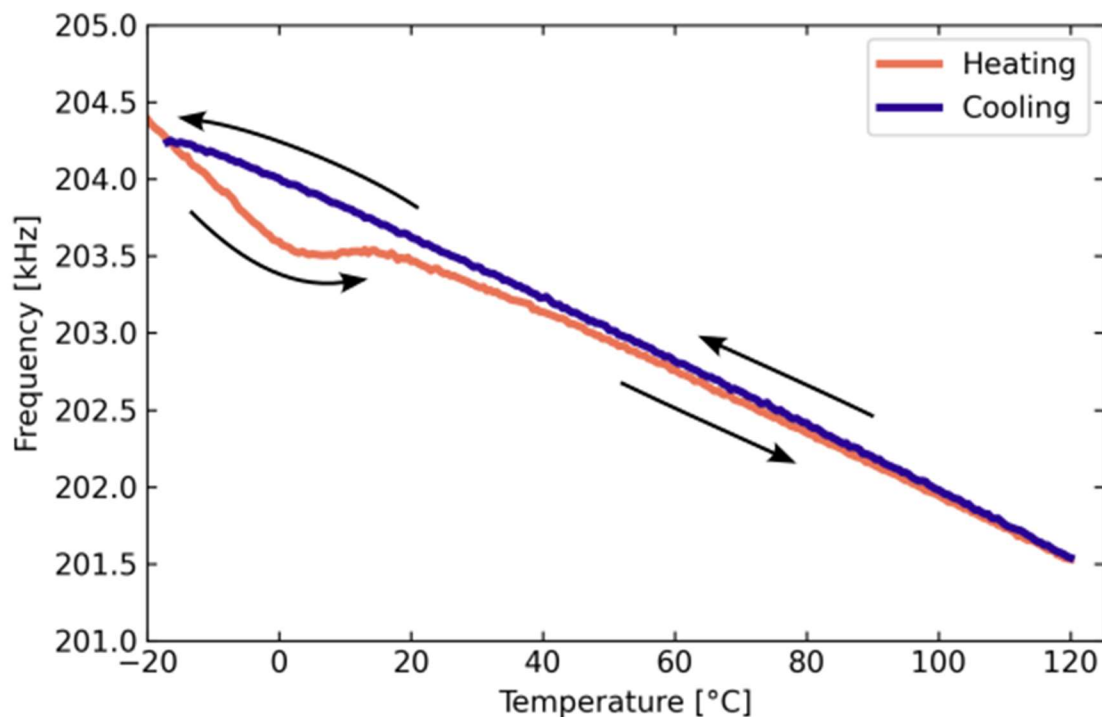


Figure 18 Anti-ferro-distortive transition of EuTiO_3 detected by resonance frequency measurements when heating or cooling the sample. Extracted from reference [v].

This experiment shows how mechanical measurements could take signs on the change of the physical properties of oxide materials. This is one example of what we call “*Oxide nanomechanics*”, meaning to study the physical properties of oxides using micro&nanomechanical structures.

Another interesting case is that represented by the ferromagnetic transition of the $(\text{La,Sr})\text{MnO}_3$ phase (LSMO). We detect the magnetic transition as a kink on the temperature dependence of the resonance frequency of a microbridge realized from a 100 nm thick LSMO film deposited on a $\text{SrTiO}_3(110)$ substrate as those reported in Figure 4. $(\text{La}_{0.7},\text{Sr}_{0.3})\text{MnO}_3$ is characterized by a magnetic transition located slightly above room temperature, at about 80 °C, that can be detected by measuring its resistance versus temperature characteristics.

The well-known Resistance vs Temperature plot is reported in **Figure 19** together with the simultaneous measurement of the first flexural mode frequency with increasing temperature. The

resistive behavior of LSMO is related to the (low-T) ferromagnetic- (high-T) paramagnetic transition that onsets at around 60 °C, while the film remains metallic.

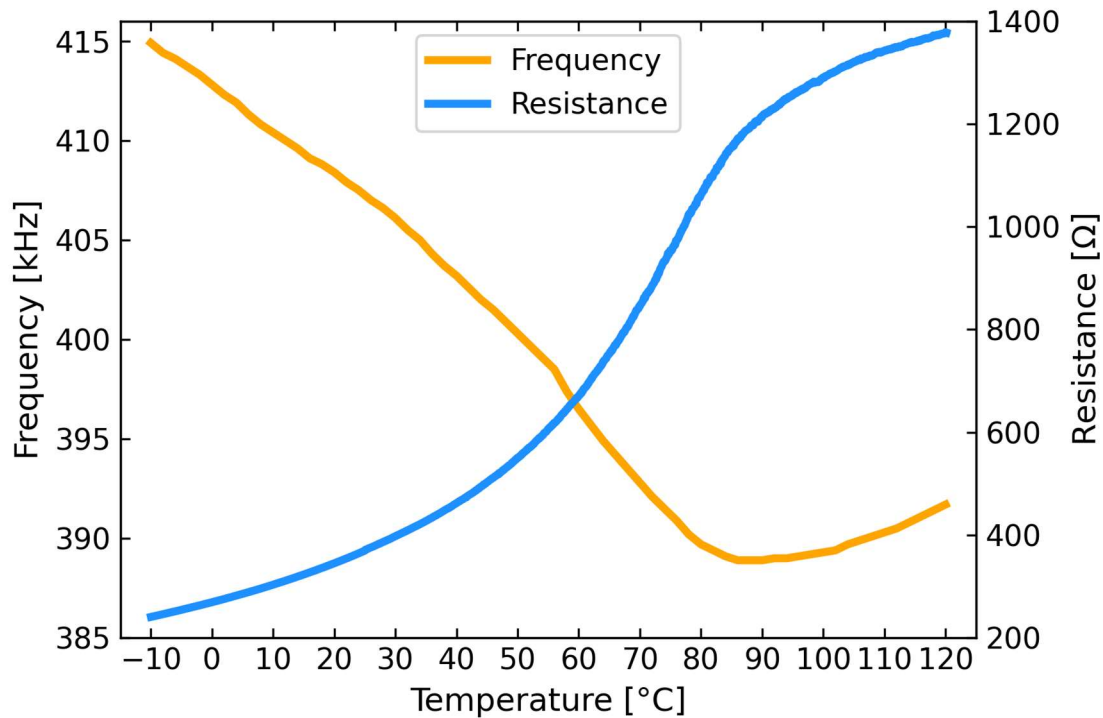


Figure 19 Temperature dependence of the electrical resistance and resonance frequency (first flexural mode) of a LSMO microbridge.

The high change of the electrical resistance with temperature suggested to use LSMO as thermal detector (bolometer), meaning to convert the absorbed heat (for example that generated by absorbed infrared radiation) into a corresponding increase of temperature that is readout electrically by measuring the instantaneous value of the electrical resistance [viii]. A freestanding object, such as these LSMO microbridges, does not dissipate heat with the substrate being this mechanism the major source of thermal dissipation. This allows for a quite generous increase of temperature with a minimal source of incident radiation and thus to a potential high-sensitivity device. The observed kink and the change of the slope of the mechanical measurement of **Figure 19** is clearly associated with the magnetic transition but its interpretation is more subtle. As from **Equation 2**, if the stress can be extracted considering a simple string model, the stress itself depends on the amount of mechanical deformation and on the intrinsic material properties, or more quantitatively $\sigma = E \cdot \varepsilon$, where ε is the deformation and E the Young's modulus. It is easy to understand this formula considering the different elongation of a polymer or stainless steel wire sustaining the same weight. In our specific case, deformation of the microbridge is not directly measurable and it is also temperature dependent because it depends on the different thermal expansion of LSMO and the substrate across the investigated temperature range (consider for example what happens to a glass bottle filled with water when cooled to 0 °C! It will break under the stress cause by the large difference in deformation of glass and water across its liquid-to-solid transition). Also, the Young's modulus can be measured only by detecting a cantilever as it has been done for ETO and straight cantilever geometries are not easily achieved with thin LSMO films. Anomalies in the value of the Young's modulus in (La,Sr)MnO₃ compounds have been measured on bulk samples with other techniques and we argue that the observed kink could be related to this. Other more focused experiments are needed to clarify

the change of slope of **Figure 19**, but, regardless the exact physical origin of the phenomenon, we are meanwhile investigating the opportunity to readout the temperature of the bridge not with an electrical measurement but measuring the resonance frequency.

OXIDE FREESTANDING STRUCTURES FOR RESONANT SENSORS

Another feature of oxide-based resonators is their possible use as detectors. Resonant sensors are widely employed in technology and nature. A mechanical resonator vibrating at one of its resonance frequency is an extremely sensitive machine. Any perturbation or change of the internal state of the resonator will likely modify the value of its resonance. For example, an added mass will change the resonance, a localized increase of temperature changes the stress and so the resonance, external forces such as electrical or magnetic interactions might change the resonance as well. It is not uncommon to be able to measure a microstructure resonating a 1 MHz and detect a change of its resonance of less than 1 Hz, meaning measuring a physical quantity with 1 part over a million! The Nanomechanical Sensing workshop series (NMC) deals with state-of-the-art sensors using these approaches.

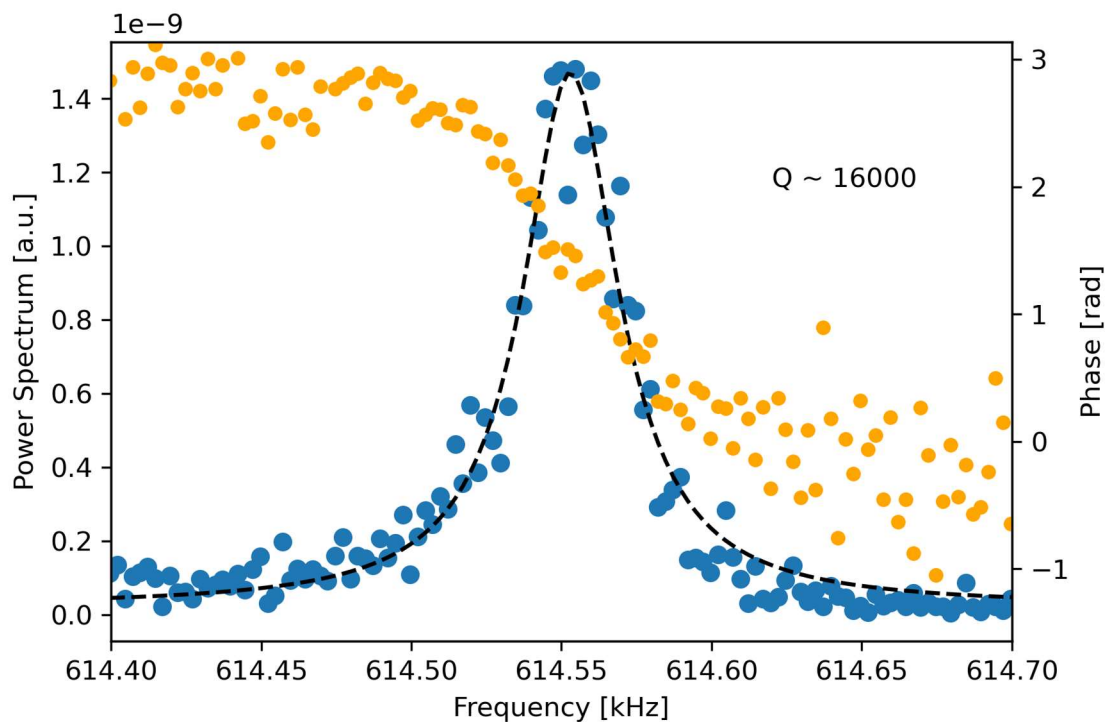


Figure 20 Resonance peak of a 120 μm long and 100 nm thick LSMO microbridge. The phase is reported in orange color, while the amplitude peak in blue color.

A fundamental parameter for the development of a resonant sensor is the mechanical Q-factor. **Figure 20** is a typical mechanical resonance centered at about 380 kHz and detected on a 250 micrometer long LSMO microbridge as those reported in Figure 4. The mechanical resonances are detected monitoring the oscillation amplitude of the resonator for a given oscillatory stimulus at a given frequency. The resonance is identified as peak in the plot, meaning that at the center of this peak the elongation of the structure for this particular mode of vibration is maximum. The peak has the typical form of a bell-shape and is analytically described by the Lorentzian function. The width of the peak at the point where the oscillation amplitude is the half of the maximum value is called “full width at half maximum” (FWHM) and is strictly related to the Q factor, which is a dimensionless parameter

defined as the ratio of the energy initially stored in the resonator to the energy lost in one oscillation. The higher the Q factor, the less energy lost during a single oscillation. The higher the Q-factor, the narrower is the resonance peak. Q-factors of the order of billions have been detected in micromechanical resonators based on silicon nitride [ix]. The energy losses of the mechanical resonators have multiple origins and might be related to the damping with air, if the resonator work in ambient conditions, or to the transmission of energy - in the form of vibrations - to the substrate via the joints or clamping points. The most dramatic effect is observed when taking out air around the resonator, especially if the structure is resonating with quite a large amplitude like the case of cantilevers and microbridges that have also low mass (lower effects are observed for bulk resonances of solids). Here, the Q factor may easily increase by a factor of one thousand. When air is removed, the Q factor is limited by the energy losses inside the material and at its surfaces.

Regardless its physical origin, resonant detectors need a high Q-factor – or a peaked resonance curve - to precisely detect the value of the resonance and its consequent shift with the external stimulus.

Measuring the Q-factor in oxide resonators, and understand how to improve it, is thus of paramount importance for the development of oxide nanomechanics comprising fundamental experiments on oxide films and the realization of sensors. We detected a value of about 50000 for the case of LSMO microbridges kept at room temperature in vacuum conditions (pressure = 2×10^{-5} mbar). The observed value has margins for improvement as we are probably limited by dissipation at the microbridge surfaces that may be contaminated during the fabrication process.

The Q-factor of our oxide microbridge is increased by tensile strain. Our experiments on LaAlO_3 microbridges show that they have in-plane tensile stress of about 350 MPa and the Q-factor linearly increases with the bridge length [x]. An intrinsic Q-factor can be thus calculated and compared with other materials, giving further hints on the dissipation mechanisms at the nanoscale.

INTEGRATION OF OXIDES FOR MULTIFUNCTIONAL M/NEMS

The fabrication processes developed during the OXiNEMS project and the measurements performed on microresonators made with a single oxide film are the beginning of an exciting journey aimed at the creation of mechanical structures composed of different layers having specific functions and all contributing to the overall mechanical behavior of - for example - a given resonator. As previously reported, many oxides have compatible structure so their integration is generally feasible. This constitutes one of the characterizing elements of oxide nanomechanics and certainly a route we will undertake in the future. Freestanding oxide heterostructures can be a valid tool for the fabrication of structures with engineered strain and strained layers (for example integrating oxides with different lattice parameters) or for the realization of devices where a specific layer interacts with the external environment. The integration of different materials requires developing fabrication processes that are compatible with all the layers and generally require the use of selective chemical etching procedures. In some cases, deposition of a second layer on top of a freestanding structure has been reported. As an example, YBCO is very sensitive to chemicals and easily destroys when in contacts with acids. To solve this problem, we prepared LaAlO_3 microbridges (insulating) and used the same as templates for the deposition of YBCO thin films by Pulsed Laser Deposition. The YBCO film grows over the entire sample and the microbridge. The sensitive layer is thus the last one in the fabrication process and does not interact with chemicals. The deposition of YBCO and other oxides is generally

optimized on bulky substrates and so the quality of the oxide layers deposited on freestanding structures need to be carefully assessed. A way to prove the quality of the deposition is to measure the electrical resistance of the microbridge as a function of temperature. The onset of superconductivity starts at $T_{C,ON}=90$ K, reaching zero resistance state at around $T_{C,0}=78$ K. The superconducting transition is broader than that obtained for YBCO films grown on the reference substrate (SrTiO_3), but optimization of the process is still underway.

CONCLUSIONS

The union of the broad spectrum of physical properties and the large integration capabilities exhibited by oxide materials with the advanced measurement techniques developed by the community working on optomechanics open exciting perspectives in understanding complex materials and in developing new types of sensors and actuators. If fundamental investigations may leave of their own for years to come, the development of oxide-base micro&nanoelectromechanical sensors face with the concurrence with well-established materials and related fabrication protocols.

OXiNEMS has further investigated new possibilities for the birth of a new technological line in the M/NEMS community aiming at developing sensors with integrated multiple functions. Benchmarking with silicon M/NEMS requires considering the added value of such integration and the richness of the functionalities and flexibility exhibited by oxides with respect with the cleanliness, reliability and cost-effectiveness of the silicon approach. We are now at an early stage of this technology and new applications that justify the increased effort in developing oxide M/NEMS are under analysis. Once again the oxides never cease to occupy researchers in undertaking experiments at the edge between real-world applications and fundamental material science.

BIBLIOGRAPHY

- ⁱ Haghiri-Gosnet et al. “**CMR manganites: physics, thin films and devices**” J. of Phys. D Appl. Phys. 36 (2003)
<https://iopscience.iop.org/article/10.1088/0022-3727/36/8/201>
- ⁱⁱ L. Pellegrino et al. “**All-Oxide Crystalline Microelectromechanical Systems: Bending the Functionalities of Transition-Metal Oxide Thin Films**” Adv. Mater. 2009, 21, 2377–2381
<https://doi.org/10.1002/adma.200803360>
- ⁱⁱⁱ A. Plaza et al. “**The role of etching anisotropy in the fabrication of freestanding oxide microstructures on SrTiO₃(100), SrTiO₃(110), and SrTiO₃(111) substrates**” Appl. Phys. Lett. 19 July 2021; 119 (3): 033504. <https://doi.org/10.1063/5.0056524>
- ^{iv} Nicola Manca et al. “**Anisotropic Temperature-Driven Strain Dynamics in VO₂ Solid-State Microactuators**” ACS Appl. Electron. Mater. 2021, 3, 211–218
<https://pubs.acs.org/doi/10.1021/acsaelm.0c00776>
- ^v Nicola Manca et al. “**Strain, Young’s modulus, and structural transition of EuTiO₃ thin films probed by micro-mechanical methods**” APL Mater. 11, 101107 (2023)
<https://doi.org/10.1063/5.0166762>
- ^{vi} J. Schiemer et al. “**Magnetic field and in situ stress dependence of elastic behavior in EuTiO₃ from resonant ultrasound spectroscopy**” Phys. Rev. B 93, 054108 (2016).
<https://journals.aps.org/prb/abstract/10.1103/PhysRevB.93.054108>
- ^{vii} Nicola Manca et al. “**Stress Analysis and Q-Factor of Free-Standing (La,Sr)MnO₃ Oxide Resonators**” Small 2022, 18, 2202768
<https://onlinelibrary.wiley.com/doi/10.1002/sml.202202768>
- ^{viii} S. Liu et al. “**La_{0.7}Sr_{0.3}MnO₃ suspended microbridges for uncooled bolometers made using reactive ion etching of the silicon substrates**” Microelectronic Engineering Volume 111, November 2013, Pages 101-104
<https://www.sciencedirect.com/science/article/abs/pii/S0167931713001251>
- ^{ix} A. Beccari et al. “**Strained crystalline nanomechanical resonators with quality factors above 10 billion**” Nat. Phys. 18, 436–441 (2022).
<https://doi.org/10.1038/s41567-021-01498-4>
- ^x Nicola Manca et al. “**Integration of High-Tc Superconductors with High Q Factor Oxide Mechanical Resonators**” <https://arxiv.org/abs/2401.12758>